The International Journal of Advanced Manufacturing Technology (2024) 134:645–656
https://doi.org/10.1007/s00170-024-14145-y

ORIGINAL ARTICLE

Dynamic modelling and efficiency prediction for forging operations under a screw press

Heyu Song[1] · Camille Durand[1] · Cyrille Baudouin[1] · Régis Bigot[1]

Received: 3 April 2024 / Accepted: 14 July 2024 / Published online: 24 July 2024

Abstract
Accurate predictions concerning a forging process can be obtained by numerical simulation, but only with a thorough knowledge of the main process variables. The material flow behavior and the interface effects are already well studied in the literature, but not the machine behavior, although it is required to estimate blow efficiency and deduce the energy actually transmitted to the workpiece. In this paper, an experimental methodology was applied to determine a spring-mass-damping model and its associated parameters for a screw press. The model and its parameters were identified with press strikes performed without billet. For validation, simulations were performed to predict blows on copper billets. The model's predictions were in good agreement with the experimental measurements for ten consecutive blows on a copper billet. The decrease of process efficiency and the evolution from inelastic blows to elastic blows were correctly depicted by the model.

Keywords Dynamic model · Machine behavior · Process modelling · Numerical simulation · Efficiency · Screw press

1 Introduction

Numerical simulation has been established as an efficient tool to optimize forging process parameters leading to a decrease in development and manufacturing time. In order to accurately anticipate the forging process by simulation, a thorough knowledge of the main process variables is required. Three different categories can be identified, related to the billet, the initial and target geometries, and the flow behavior [1]; the behavior at the billet-tools interface, i.e., thermal exchange and friction effects [2]; and the characteristics of the forging equipment and the impact of the environment on the forging process [3].

Despite an extensive literature on material and interface behaviors, in some cases, simulations do not provide a representative picture of the reality, like for a forging operation of high-performance material on an energy-driven machine of industrial size [4]. The simplification of the machine behavior in simulation is considered one of the main causes for such accuracy loss [5, 6].

✉ Heyu Song
heyu.song@ensam.eu

[1] Arts Et Métiers Institute of Technology, Université de Lorraine, LCFC, 57070 Metz, France

Screw presses are energy-driven forging machines in which the ram is driven by a flywheel delivering the amount of energy set by the operator. The kinetic energy available is directly dependent of the ram speed. Thus, while forging hammers and screw presses are both energy-driven, screw presses exhibit relatively slower ram speeds ranging from 0.5 to 1.2 m/s.

Different approaches were used in the literature to model forging presses: the elastic behavior can be considered through a stiffness matrix identified theoretically [7] or experimentally [8], possibly with specially designed tools [9]. For a multi-stage process on a mechanical press, the influence of the press and tool deflections on the workpiece was investigated [10]. For an extrusion process, the equivalent press stiffness was determined according to experimental German standards and the tool stiffness was determined by simulations using finite element methods (FEM) [11]. More recently, in the case of mechanical presses, hybrid models were developed. A coupled multi-body system and a finite element simulation (MBS-FEM) for sheet metal forming applications was established [12]: a mass was attributed to each element of the press, connections between elements were defined, and the behavior of the machine was then coupled with the FE simulation of the sheet stamping. Zheng et al. [13] also proposed a hybrid model considering the elastic behavior of the crankshaft using FE and resulting

in a rigid-flexible coupling of the model of the slider crank mechanism.

These models are successful for slow-forming processes, but they do not consider the dynamic effects that are significant for screw presses as well as forging hammers. A dynamic model of the hammer foundation was proposed in [14] and was recently extended to take into consideration base isolators [15] as this may have an impact on maximum blow force. More recently, the foundation of a forging hammer was analyzed and modeled in order to control and dampen the vibrations [16]. These methodologies are based on theoretical knowledge of the machines and their foundations and not on experiments, as the instrumentation of such forging machines raises difficulties. But nowadays, modern measurement systems facilitate the monitoring of forging processes even for hot forging operations [17]. Indeed, Galdos et al. [18] and Chen et al. [19] were able to determine the impact velocity of a counterblow hammer in the case of copper upsetting thanks to high-speed cameras. For an aluminum hot forging operation on a screw press, radar sensors were used to measure ram tilting and frame stretching [20]. In the case of stamping operations, different sensor positions and measuring methods were tested and compared to measure the process force [21]. Saberi et al. measured the ram velocity with a laser velocity meter and the ram acceleration with an accelerometer sensor for a steel hot forging operation on a hammer [22]. Here, both theoretical and experimental investigations were carried out to model the mechanical vibrations of the hammer.

In this paper, an experimental methodology to identify the best-suited spring-mass-damping model for a screw press is developed and applied. The method allowing to model the machine and its tools and identify the associated parameters is shown in Section 2. Section 3 exhibits the comparison of experimental and simulated results in the case of several consecutive blows on a copper cylinder. Energy repartition and efficiency at each forging blow are discussed in Section 4.

2 Experimental and numerical methods

2.1 The screw press, its tools, and sensors

The screw press under study is the LASCO SPR 400 from the Vulcain platform in Metz, France (Fig. 1). The press has

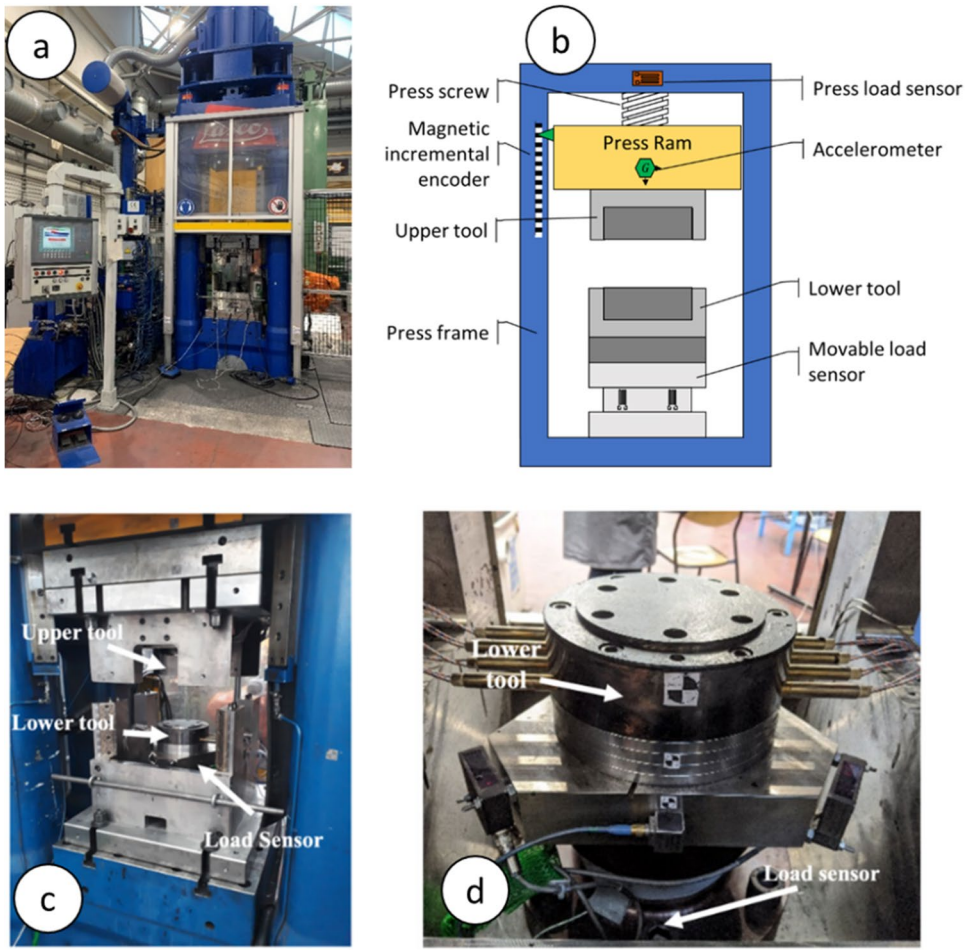

Fig. 1 **a** The screw press; **b** the schematic of the press, tools, and embedded sensors; **c** the instrumented forging tool; and **d** the movable load sensor and the lower die

a portal frame structure and is equipped with a direct electric drive motor providing the forging energy [4]. The press can deliver a maximal energy of 28.9kJ with a maximal speed of 680 mm/s. A toolholder is mounted on the press with flat dies as forging tools: the upper toolholder is fixed to the ram, and the lower toolholder is fixed to the bedplate of the press.

As the objective of the study is to experimentally determine a dynamic model of the press and its tools, several sensors were embedded either in the press or in the tools to record load and displacement data. First of all, the press is already equipped with a magnetic incremental encoder (MW991424 from IPF Electronic) recording the displacement at ram speeds up to 5 m/s with a resolution of 10 µm. A load sensor (HBM SLB-700A/06VA1) is located on the crosshead of the press and is devoted to press piloting rather than press monitoring. Thus, a movable load sensor made by Doerler and constituted of strain gauges is embedded in the lower toolholder to accurately record the load close to where the forging strikes take place. This load sensor can measure up to 6300 kN and has a stiffness of 3.39×10^{10} N/m. In addition, a triaxial capacitive accelerometer (Kistler 8396A050) is fixed to the ram of the press to be able to measure the ram acceleration during blows [23].

2.2 Experiments

Three cylindrical copper billets were upset at room temperature under the screw press without any lubricant. The same forging procedure was repeated three times on three identical copper billets to check the repeatability of the process (Table 1). Each billet was struck ten times, each time at 25% of the 28.9 kJ maximal press energy. Ten consecutive blows were realized, in order to cover the transition from inelastic collision to quasi-elastic collision which is needed to record the elastic behavior of the press. The inelastic collision occurs at the first blows when the kinetic energy is mainly absorbed by the plastic deformation of the billet, whereas the quasi-elastic collision occurs when the kinetic energy is mainly dissipated in elastic energy in the press. Copper was selected because it can be forged at room temperature with the selected equipment. In this way, thermal effects on the material flow stress can be neglected. Moreover, Dao et al. [24] have shown that strain rate has only little influence on the copper flow stress allowing to neglect the strain rate effect on the flow stress in the billet modelling.

A number of bare strikes, without billet, with tool against tool were also performed with an energy of 28% of 28.9 kJ as it is the maximum amount of energy allowed in those conditions. Bare strikes ensure a purely elastic collision; thus, these strikes were used to identify the dynamic model, whereas the strikes with billet were used to validate the model.

2.3 Dynamic model of the production system

The objective of the study is to determine a dynamic parametric model with a mass-spring-damper of the production system constituted of the screw press and its tools during the forging operation. In a generic way, a mass-spring-damper model is structured as shown in Fig. 2 [25].

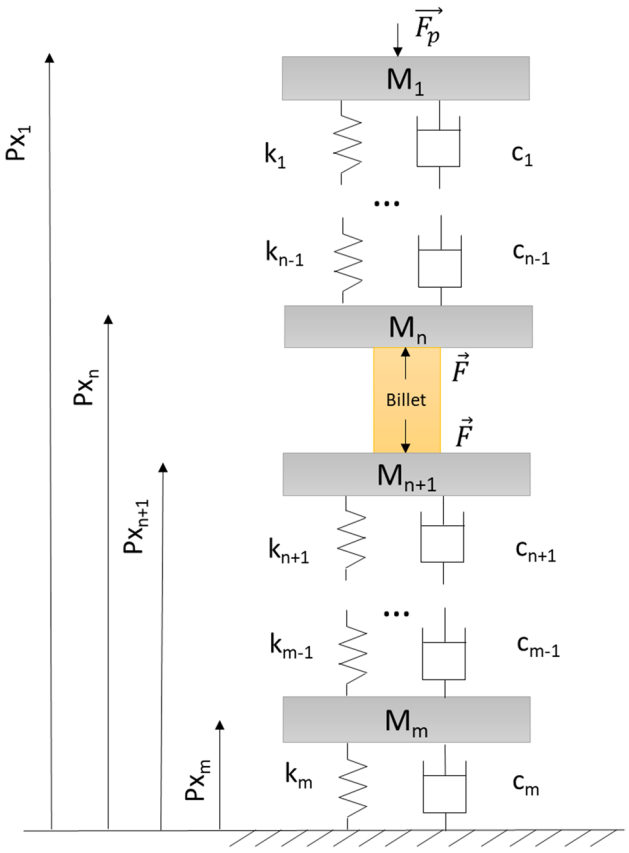

Fig. 2 Schematic of the general dynamic model with masses, springs, and dampers for a forging machine

Table 1 Billet characteristics and experimental settings

Billet material	Number of billets	Billet diameter (mm)	Billet height (mm)	Energy per strike (kJ)	Impact speed (m/s)	Number of consecutive strikes	Lubricant
Cu99%	3	49.8	30	7.45	0.346	10	no

The application of the fundamental principle of the dynamics to the masses provides the dynamic equations of the press system which can be written in matrix form as

$$M \cdot \ddot{X} + C \cdot \dot{X} + K \cdot X = \overrightarrow{F_p}, \tag{1}$$

where $\vec{X}$ designates the displacement vector for every mass, $\boldsymbol{M}$ the mass matrix, $\boldsymbol{C}$ the damping matrix, $\boldsymbol{K}$ the stiffness matrix, and $\vec{F}_p$ an external force that can be applied on the masses, depending on the machine considered. The force $\vec{F}$ applied by the billet on the masses M_n and M_{n+1} is a function of the displacement of the masses directly in contact with the billet (X_n and X_{n+1}) and is defined as

$$\vec{F} = \gamma\left(X_n, X_{n+1}\right).\overrightarrow{F_L}\left(X_n, X_{n+1}\right) \tag{2}$$

with F_L the forging load depending on the material behavior and that is deduced from finite element (FE) simulation as further explained in Sect. 2.4, and γ the contact coefficient defined as.

$$\begin{gathered}\gamma = 1 \; if \; at \; t = i, (X_n - X_{n+1})_i = \min\left(X_n - X_{n+1}\right)_{i-1} \\ \gamma = 0 \text{ otherwise}\end{gathered} \tag{3}$$

The γ coefficient allows to consider the period of contact losses due to vibrations and during which the billet does not exert any action on masses M_n and M_{n+1}.

In order to determine the adequate dynamic model of a specific production system, this one is put under a forging condition, and the forging load F_L is recorded thanks to the load sensor embedded in the tool and is analyzed with a fast Fourier transform (FFT) to determine the number of frequency peaks corresponding to the minimum number of degrees of freedom (DoF) of the model [25]. Based on the FFT results and knowing the boundary conditions of our system, a mass-spring-damper model is defined and the model's parameters are then identified thanks to numerical optimization methods. In our case, the boundary conditions correspond to the ram velocity before the impact, deduced from experiments, which was equal to − 0.363 m/s for bare strikes and to − 0.346 m/s for the blows on billet. The movable load sensor embedded in the lower tool is modeled as a spring with a stiffness of $k_s = 3.39 \times 10^{10}$N/m according to the supplier. The objective function used to determine simultaneously the loading and the spectral error between experimental and simulated data was as follows:

$$OF(F,S) = f \cdot g\sqrt{\frac{1}{n}\sum_{i=1}^{n}\frac{\left(F_i^{exp} - F_i^{sim}\right)^2}{F_i^{exp\,2}}} + (1-f)\cdot(1-g)\sqrt{\frac{1}{m}\sum_{i=1}^{m}\frac{\left(S_i^{exp} - S_i^{sim}\right)^2}{S_i^{exp\,2}}} \tag{4}$$

where OF is the objective function, F^{sim} is the simulated load value at the spring k_s, F^{exp} is the load measured by the movable load sensor embedded in the tool, S^{sim} is the simulation spectrum value, S^{exp} is the experimental spectrum value, n and m are respectively the number of measurement points and the number of effective frequencies of the spectrum, $f = m/(m+n)$, and g represent the weighting coefficients of the load spectrum in the objective function. Here, after several optimizations, $g = 0.5$ was taken. The value of the objective function is calculated and compared to the convergence criteria, and it is further minimized by changing the model parameters. The model was implemented in a Python program, and the parameter identification was realized using a gradient descent method. With this method, an initial set of parameters has to be given to facilitate the convergence of the objective function. The initial set of parameters was based on the physical characteristics of the system. For example, the mass values were based on M_{eq}. Indeed, for a screw press, the available forging energy can be expressed with the equivalent moving mass (M_{eq}) and the velocity of the ram before the impact (V_0) as defined in Eq. (5).

$$E_0 = {}^1\!/_2 . M_{eq} . V_0^2 \tag{5}$$

In the case of the presented press, M_{eq} is equal to 125,000 kg. Thus, mass 1 and mass 2 were defined so that their summation is equal to M_{eq}, and with mass 2 lower than mass 1, as mass 2 is related to the tools. M_1 was equal to 120,000 kg and M_2 to 5000 kg. Moreover, a previous study [4] has shown that the static press stiffness had a value of around 2×10^9 N/m, and thus, this value was taken as an initial parameter for both k_1 and k_2. Finally, the initial damping coefficients were taken equal to 2×10^5 N.s/m after empirical value trials. The algorithm will iterate to minimize the value of the objective function starting with the set of initial parameters defined.

2.4 Simulation of the billet forging

The response of the copper billet subjected to a displacement of the two tools was simulated with the FE method, using the software Forge NxT 3.2. Thanks to its well-known rheology, the literature often refers to cold copper upsetting in order to characterize machine's behavior [26]. Therefore, the copper material's behavior was selected from the software database and is described by a constitutive law of Hansel Spittel:

$$\sigma_f = A \cdot e^{m_1 T} \varepsilon^{m_2} \dot{\varepsilon}^{m_3} e^{m_4/\varepsilon} \tag{6}$$

where A, m_1, m_2, m_3, and m_4 are coefficients determined for the Copper, T is the temperature, σ_f is the material's flow stress, ε is the equivalent strain, and $\dot{\varepsilon}$ is the equivalent strain rate during the deformation. The values of the coefficients for copper at room temperature are taken from the Forge NxT 3.2 database and are given in Table 2. As variabilities in the billet properties still can exist, it can

generate uncertainties. But these uncertainties will only have an impact on the maximal forging load, the forging time and the final billet height. Indeed, if the copper flow stress is overestimated, it would result in less billet deformations, thus a higher final billet height and a shorter forging time with a lower maximal forging load.

The room temperature was set to 20 °C, and thermal exchanges with air and tools were considered with heat transfer coefficients equal to 10 kW.m^{-2}.K^{-1} as it corresponds to a moderate heat exchange with a cold steel according to Forge's NxT 3.2 database. The friction was modeled with a Coulomb limited Tresca law, frequently used for forging processes in the literature [27–29] with $\mu = 0.05$ and $\overline{m} = 0.1$ as the literature indicates a friction coefficient for copper varying between 0.05 and 0.15 [3, 30, 31]. Tetrahedral elements with an average size of 2.3mm were chosen for the mesh. Elastic and damping effects due to the machine-tools system were not considered in this simulation.

The FE simulation and the dynamic model are only weakly coupled: the FE simulation is only used to provide the material behavior. Indeed, thanks to the FE simulation the forging load as a function of the billet height for the interval from 30 to 5 mm is obtained as shown in Fig. 3. Knowing the displacement of the masses thanks to the dynamic model, the billet's deformation is deduced, and the prediction of the required forging force comes from the FE simulation. If there is no billet during the strike, no FE simulation is required and this step can just be ignored.

3 Results and discussion

First, blows without billet were analyzed (Sect. 3.1) in order to identify the dynamic model of the press-tools system (Sect. 3.2). Subsequently, the model was used to simulate blows with billet as an application case to validate the model (Sect. 3.3) and explore its predictions in terms of energy repartition (Sect. 3.4).

3.1 Bare strike experimental results

Figure 4 shows the evolution of the load for three bare strikes. All the curves are overlapping, and the average of the maximum load value is equal to 5550 kN with a variation range of 2.4 kN, meaning a relative standard range (RSR), defined as the ratio of the range on the average value, equal to 0.04%. The

Table 2 Coefficients of the Hansel Spittel law for the cold copper (database Forge NxT 3.2)

A(MPa)	m_1	m_2	m_3	m_4
411.19	−0.00121	0.21554	0.01472	−0.00935

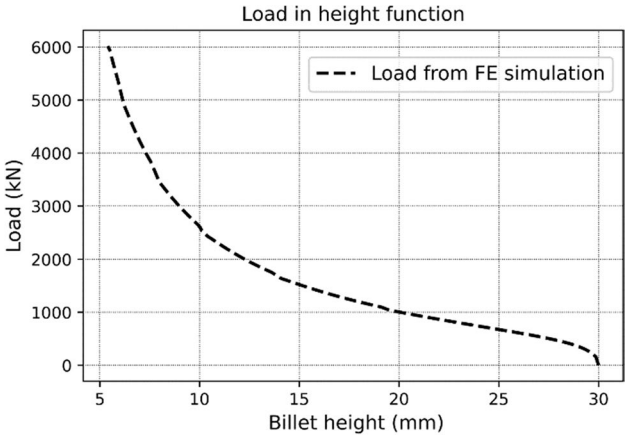

Fig. 3 Load F_L as a function of the billet height from the FE simulation

experiment is found repeatable; thus, in the following, only one strike will be shown for clarity.

The time evolutions of the load and ram displacement are shown in Fig. 5. The ram displacement is counted in the opposite direction of the strike direction. The acceleration signal allows to determine the time at which the strike begins.

An FFT analysis was realized on the load signal from the movable load sensor. The resolution of the FFT spectrum δf calculated according to the length time of the signal (t_{exp}) was equal to $\delta f = 1/t_{exp} = 36.4$Hz. The spectrum is shown in Fig. 6a. The frequencies identified with the FFT are sorted from the highest to the lowest amplitude, and a Pareto chart is drawn in Fig. 6b.

The dominant frequencies of 0 Hz, 36.4 Hz, and 292 Hz explain more than 80% of the signal information. The

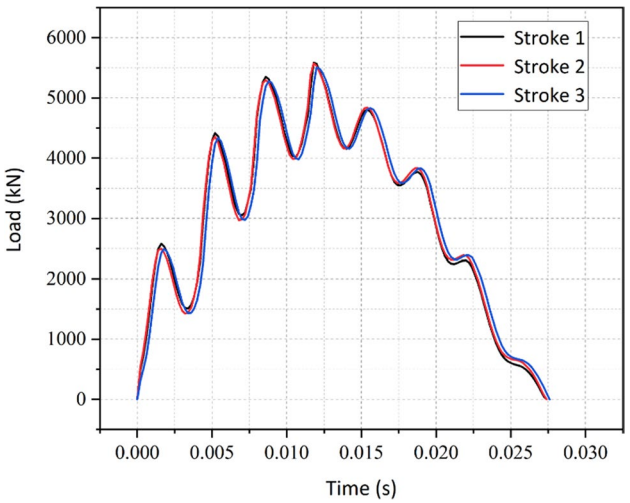

Fig. 4 Load in the function of time for the three blows without billet

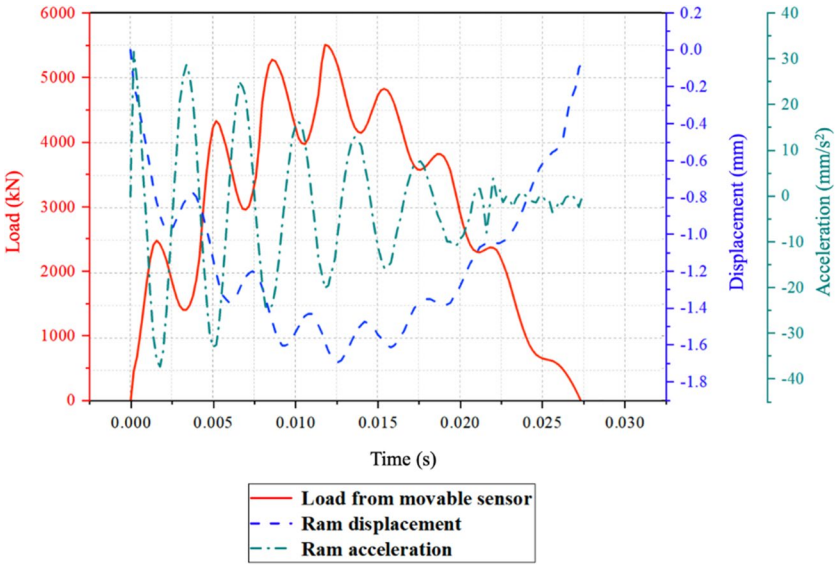

Fig. 5 Ram's load, acceleration, and displacement in function of time for one blow without billet

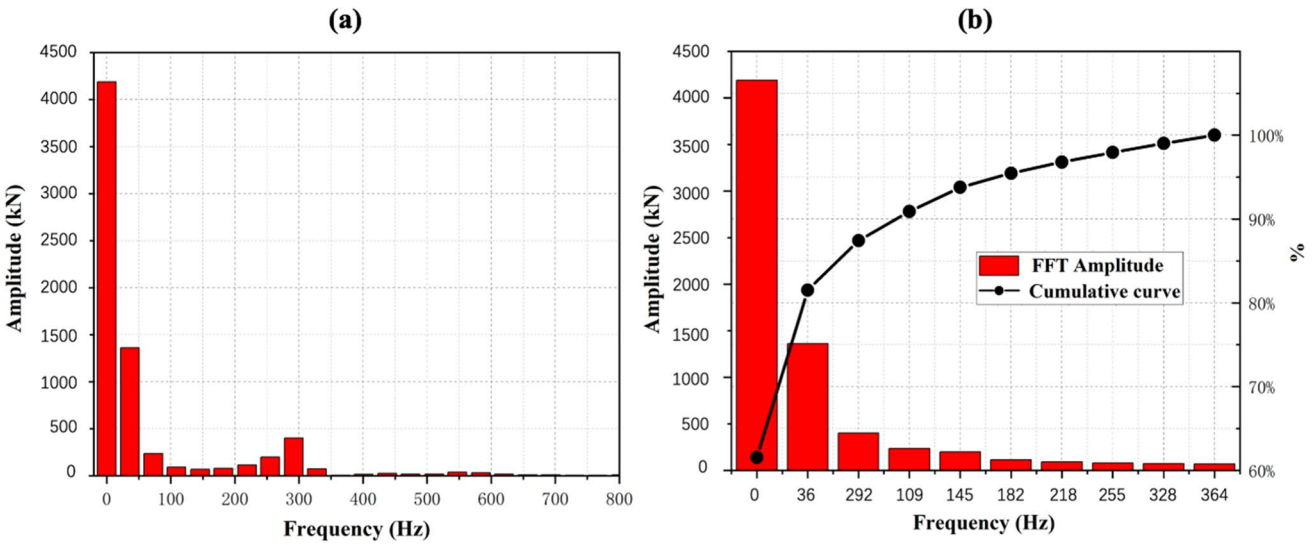

Fig. 6 **a** FFT of the load for a bare strike and **b** Pareto chart on the amplitudes of the frequencies from the FFT

frequencies of 0 Hz and 36.4 Hz correspond to the same vibration mode, but it is impossible to clearly identify the associated frequency. Indeed, it can be seen in Fig. 5 that only half of the period of the carrier wave corresponding to the frequencies of 0 Hz and 36.4 Hz is recorded during the experiment. Thus, the FFT does not allow to identify this frequency. The second frequencies of 292 Hz seem to be related to the tools as the value of this frequency changes by changing the tool mounted on the press. So, even if the exact frequency of the carrier wave cannot be identified, the FFT highlights the existence of two main vibration modes in the load signal: a low frequency near 0 Hz and a second one at about 292 Hz. Therefore, only these two vibration modes will be considered in the model, as described in the next section.

3.2 Dynamic model identification

According to the FFT analysis, a two-degrees-of-freedom spring-mass-damping vibration model is proposed to describe the press behavior during the shock (Fig. 7). This model is constituted of two masses, two dampers, and two springs in addition to the movable load sensor's spring. The spring k_1 and the damper c_1 model the elastic deformations and the damping effects of the machine frame which is fixed on the ground. On top of c_1 and k_1, the load

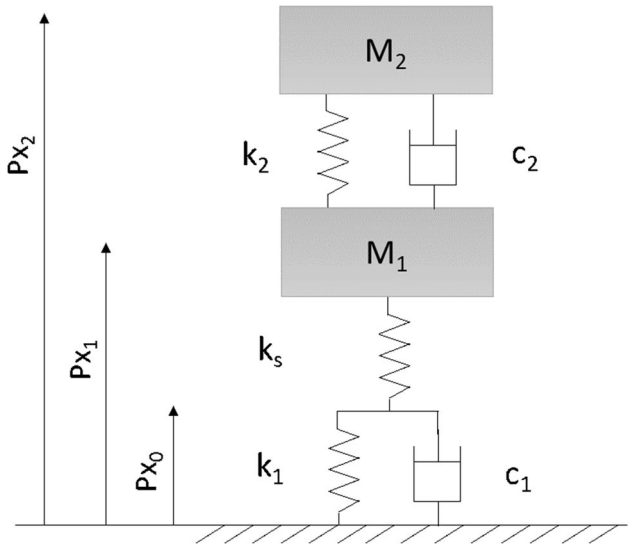

Fig. 7 Model of the screw press with the embedded load sensor in the lower tool in the case of a bare strike

sensor embedded in the lower tool is modeled by the known spring k_s. During the shock, this spring is in contact with the sub-system composed of masses M_1 and M_2 that represent the upper moving parts of the system (upper tool, upper toolholders, ram, screw, flywheel). The spring k_2 and the damper c_2 link the two masses and model the elastic deformations and damping effects between the moving parts of the system.

The application of the fundamental principle of dynamics to the masses M_1 and M_2 provides the dynamic equations of the press system as presented in Eqs. (7), (8), and (9).

$$\boldsymbol{M_2\ddot{X}_2 = -k_2\left(X_2 - X_1\right) - c_2(\dot{X}_2 - \dot{X}_1)} \tag{7}$$

$$\boldsymbol{M_1\ddot{X}_1 = k_2\left(X_2 - X_1\right) + c_2(\dot{X}_2 - \dot{X}_1) - k_s\left(X_1 - X_0\right)} \tag{8}$$

$$\boldsymbol{-k_s\left(X_1 - X_0\right) = -k_1X_0 - c_1X_0} \tag{9}$$

with X_1 the displacement of the mass 1, X_2 the displacement of the mass 2, and X_0 the displacement of the upper point of the spring k_1 with respect to their respective position at $t=0$. The same initial velocity equal to -0.363 m/s is assigned to the mass 1 and the mass 2 at $t=0$. This velocity corresponds to the experimental measurement of the ram velocity before the impact. The stiffness k_s of the movable load sensor is fixed to 3.39×10^{10} N/m according to the sensor documentation.

Thanks to a numerical optimization method, the model parameters were identified (Table 3) and the load at k_s as well as the FFT on the load was simulated, plotted, and compared to experimental data (Fig. 8).

Table 3 Values of identified parameters

M_1	106,000 kg
M_2	3110 kg
c_1	0 N.s/m
c_2	3.61×10^5 N.s/m
k_1	9.74×10^9 N/m
k_2	1.72×10^9 N/m

The objective value was equal to 0.545 with these identified parameters. Concerning the masses obtained, the summation of the mass 1 and mass 2 gives an equivalent mass model equal to 109,000 kg, meaning a relative deviation of 13% with M_{eq}, but the order of magnitude remains correct. Even though, the masses identified are modal masses and thus do not have to correspond exactly to the physical masses. For the stiffnesses, both values are in the same order of magnitude of 10^9 N/m, like the initial parameters, but k_1 is nine times higher than k_2. The damping coefficient c_2 is found to be close to its initial value, whereas c_1 is null. These results are quite logical as the heaviest mass M_1 is associated with the highest stiffness and no damping, whereas the lowest mass M_2, probably related to the tools, is less stiff but has damping effects.

It can be seen from Fig. 8a that the simulated and experimental load follows a similar trend, with the same duration of blow, and there is only a relative deviation of 9.05% comparing the maximum experimental load of 5490 kN, to the simulated one of 4993 kN. Actually, the simulated signal fits better than the experimental signal after they have reached the maximum blow force.

3.3 Application to billet upsetting

Once the production system's model was identified, it was tested for the application case with strikes on copper billets. Thus, the dynamic model was updated to include the billet (Fig. 9). During the forging process, the load $\vec{F}$ is imposed by the billet to the mass 1 and to the spring k_s, according to the billet rheological behavior.

Applying the fundamental principle of dynamics again, the system's equations of motion are obtained:

$$M_2\ddot{X}_2 + k_2\left(X_2 - X_1\right) + c_2\left(\dot{X}_2 - \dot{X}_1\right) = 0 \tag{10}$$

$$M_1\ddot{X}_1 - k_2\left(X_2 - X_1\right) - c_2\left(\dot{X}_2 - \dot{X}_1\right) = -\vec{F} \tag{11}$$

$$-k_S\left(X_s - X_0\right) = \vec{F} \tag{12}$$

$$-k_S\left(X_s - X_0\right) = -k_1X_0 - c_1X_0 \tag{13}$$

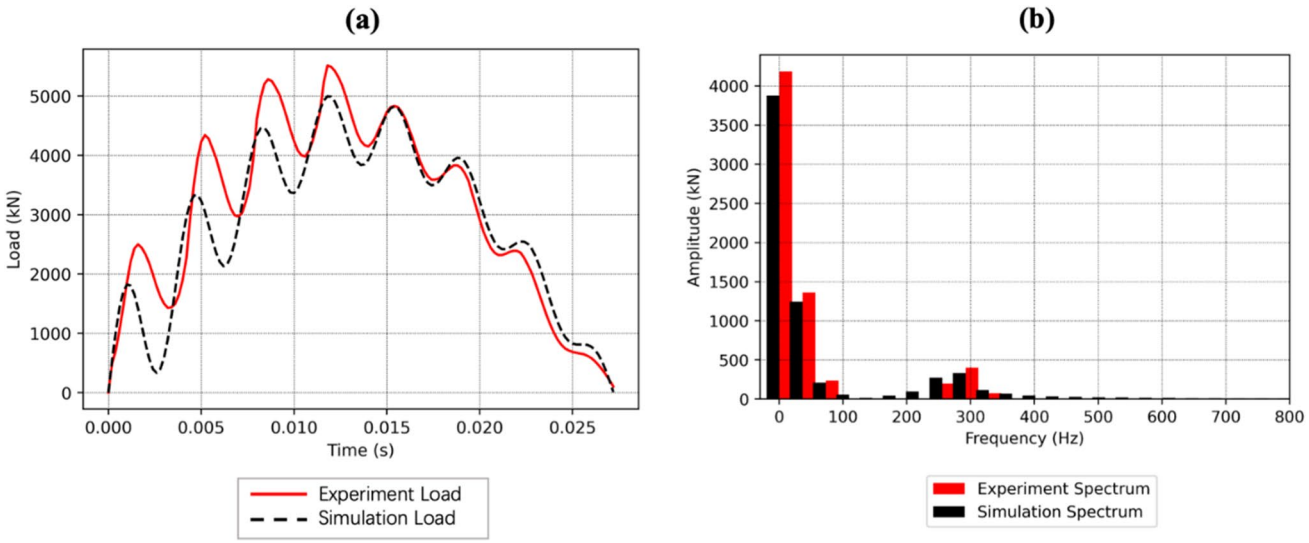

Fig. 8 **a** Evolution of the experimental load from the movable sensor and the simulated load for k_s. **b** Spectrum of experimental load from the movable sensor and the simulated load for k_s

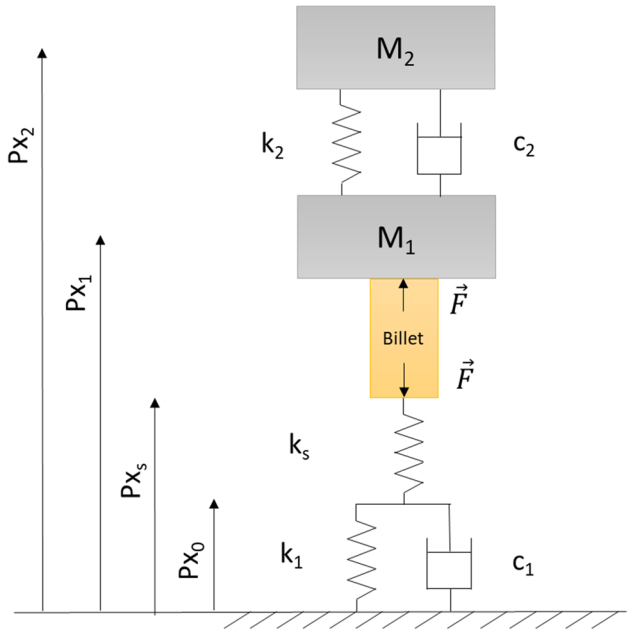

Fig. 9 Coupled model considering machine and billet behavior

The load measured by the movable sensor and the simulated load for k_s for a first upsetting blow are shown in Fig. 10. As for bare strikes, the blows on the three billets were repeatable; thus, for clarity reason, the results obtained on only one billet are presented. During the forging process, the simulation slightly overestimated the load compared to the experiment. The maximum predicted blow force was 1124 kN, which is 2.74% higher than the measured value (1094 kN). The forging time, defined as the time to reach the maximum blow force, is equal to 52.2 ms in experiment and 55.8 ms in simulation giving a relative deviation of 6.4%. After reaching the maximum blow force, differences are observed between simulation and experimental results concerning the spring-back time: the simulated one is equal to 12.5 ms whereas the experimental one is 17.2 ms.

Figure 10 also shows the ram displacement obtained by experimental measures and by simulation. Until reaching the maximum blow force, the simulation overestimates slightly the ram displacement with a maximum relative deviation of 7.53%.

The model was further used to simulate several blows on the billet. Figure 11 shows the evolution of the simulated load carried by the load sensor k_s for ten consecutive blows and load measured by the movable sensor. For every simulation, the initial velocity of the masses M_1 and M_2 was − 0.346 m/s. The load simulated for the first blow is drawn, and then a temporal offset is used to set the beginning of the next blow at the end of the first blow. The same manipulation is done for the other blows. After each blow, as Fig. 11 shows, with the increase of blowing times, the experimental data and simulation results have the same change pattern. The forging time decreases, and the maximum blow force increases. The vibrations associated with the 2nd vibration mode can be observed from the 2nd blow to the 10th blow. The amplitude of the 2nd vibration mode is higher with the number of blows.

The maximum experimental load per blow is an increasing function of the number of blows, but it can be noticed

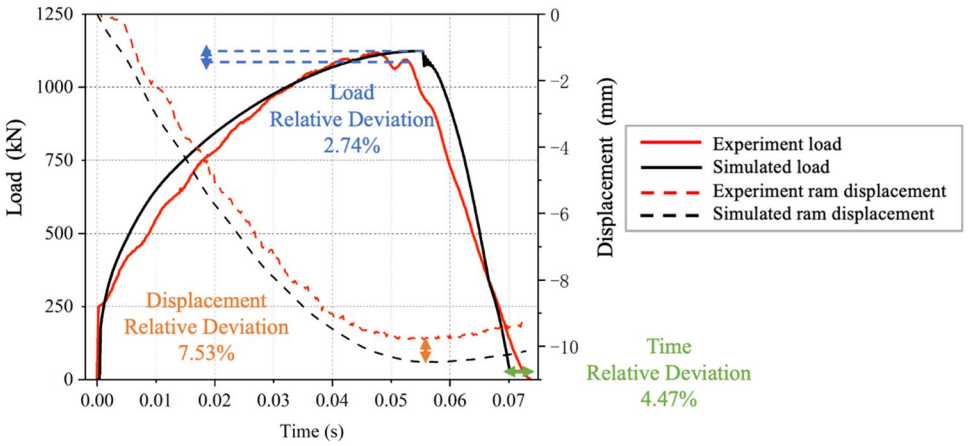

Fig. 10 Forging load and ram displacement measured by the movable sensor and press displacement sensor, load in k_s, and ram displacement simulated for the first blow of copper upsetting

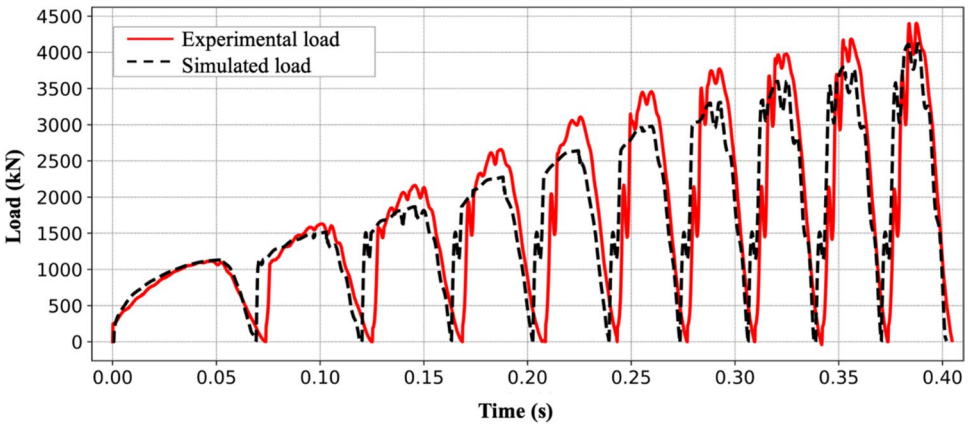

Fig. 11 Load measured by the movable sensor and load simulated in k_s for ten consecutive blows on a copper cylinder specimen

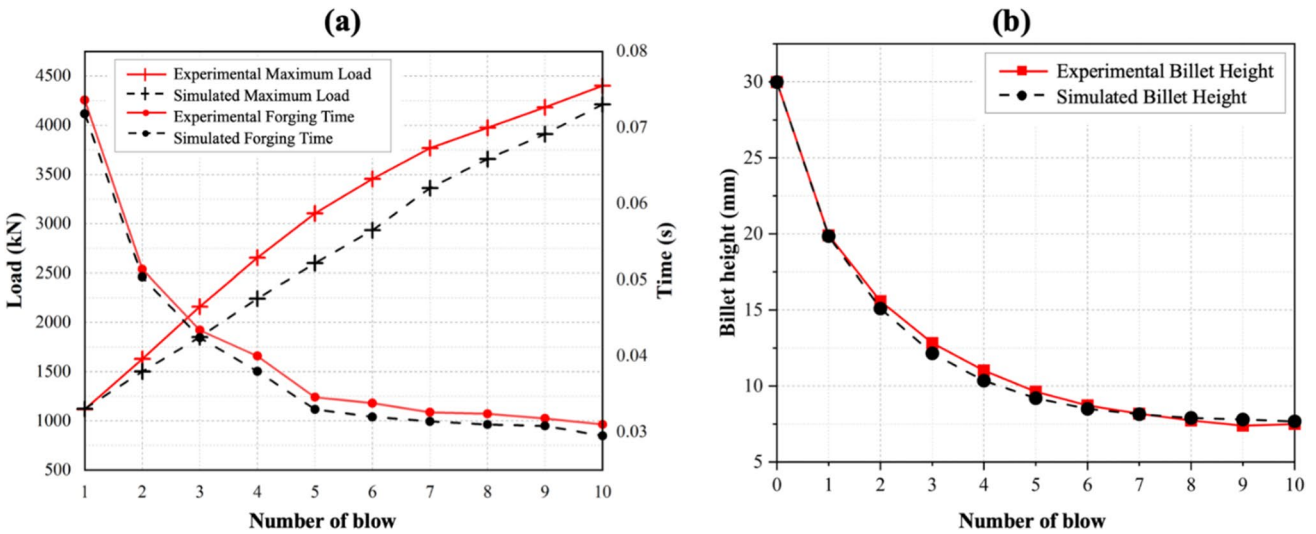

Fig. 12 **a** Experimental and simulated maximum forging load and forging time for each blow. **b** Experimental and simulated billet final height for each blow

that the growth decreases after each blow (Fig. 12a). The maximum simulation load was always smaller than the experimental data. The maximum simulation load for each blow increased uniformly with the number of blows. The relative deviation of the simulated and experimental loads gradually grows until the sixth blow, before reducing again. Concerning the forging time of the experiment, it decreases with the number of blows and exhibits an asymptotic behavior. Both the simulated and the experimental forging time have similar trends. Figure 12b shows that the billet height is a decreasing function of the number of blows and that simulated results almost overlap the experimental ones.

3.4 Discussion on forging efficiency prediction

This paper further expanded the method developed in [25] to experimentally identify the dynamic model of a forging hammer production system and applied it to a screw press system. The instrumentation differs from the one used on the hammer and allows to both monitor the process and identify the model. The model predicted well the increase of the maximum blow force and the decrease of the billet height, which was consistent with the experimental results. The dynamic model identified for the screw press system was able to correctly predict the evolution of forging load and billet height even with the accumulation of blows that could generate an accumulation error as well.

Increasing load causes more elastic deformation of the machine structure. Thus, less energy is actually transmitted to the billet at each blow and the efficiency of the forging process decreases. Indeed, for each blow, the input kinetic energy coming from the motion of the two masses is turned into four types of energy: the plastic energy consumed to plastically deform the billet, the friction energy dissipated at the interface between tools and material, the elastic energy stored by the springs, and the damped energy dissipated by the dampers. The repartition of the energy of the system for each forging blow can be calculated thanks to the spring-mass-damping model coupled with the billet model, as shown in Fig. 13. The forging efficiency is defined as the ratio of the plastic energy transmitted to the billet on the input kinetic energy. For the first three blows, the kinetic energy was mainly transformed in plastic deformation of the billet. However, while the efficiency was high for the first blows (87%), it decreased significantly after each blow to reach the value of 25% for the 10th blow.

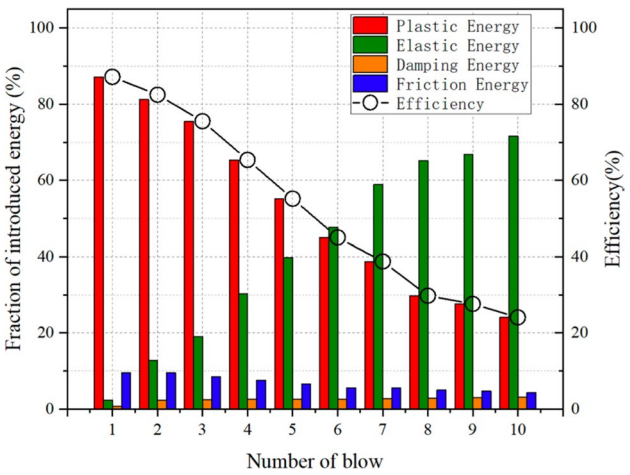

Fig. 13 Distribution of the energy and process efficiency for ten simulated blows on a copper billet

The friction energy slightly decreased over the blows but remained low as it never exceeded 10%. The damping energy remained quite small and almost constant over the blows, always representing less than 5%. The elastic energy, almost negligible at the first blows, significantly increased with the number of blows until exceeding the plastic energy at the 6th blow and representing as much as 70% at the final blow. It appears that when forging under a screw press, the billet absorbs less and less kinetic energy as plastic deformation; thus, the remaining energy is mostly dissipated in the elastic deformation of the machine and its tools.

In the literature, the question of efficiency is often discussed with the aim of optimizing a forging process or tool design. When it deals with the machine's efficiency, more often it's hammers that are taken under consideration [32, 33] and not screw presses, even though screw presses are also energy-driven machines, like hammers. Concerning the efficiency of the consecutive blows on one part with a simple geometry [34] stated that the efficiency from the first blow to the tenth was from 72 to 56% whereas for the screw press, we obtained 87 to 25%. Thus, results find here for the screw press are enlarging the efficiency range.

In order to further evaluate the interest of the developed dynamic model, finite element simulations of the same process were performed with Forge NxT, without modeling the elastodynamic behavior of the press. The screw press blows simulated with Forge NxT were significantly more efficient than in the reality and reached higher billet deformation: eventually, 5 mm final billet height was reached for the 10th blow, whereas the real deformed copper billet was 7.5 mm high. Moreover, the FE simulation did not describe the vibration modes of the machine. This highlights the interest of using such a dynamic model for screw presses and other energy-based forging machines.

Of course, by now, the developed dynamic model is only weakly coupled to the finite element simulation of the billet behavior during the forging operation. A step forward would be to implement a strong coupling between both.

4 Conclusions and outlook

This paper presents a spring-mass-damping model for a forging operation under a screw press with an experimental approach for the parameter identification. The number of degrees of freedom and the parameters associated with the model were identified thanks to bare strikes without billet. The model was then applied to copper billets upsetting at room temperature. The simulated forging load and billet height have shown good agreement with experimental measurements. Finally, the model was exploited to determine the energy distribution as well as the efficiency for each blow. The following conclusions were drawn:

1. The experimental approach to determine the dynamic model of screw press production system during a forging operation is relevant. Ram's displacement, acceleration, and load were monitored in the case of bare strike to properly identify the press-tools system.
2. The model's predictions were in good agreement with the experimental results for ten consecutive blows on a copper billet. Thus, the identified parameters are transferable to different forging operations, confirming the predictive capacity of the model.
3. Based on the model, the energy distribution in the system can be represented as well as the efficiency for each blow. The model was able to accurately simulate the transition from inelastic to elastic blows with the decrease of the process efficiency and highlights the preponderance of the elastic energy losses. Thus, the model could be used as a decision support tool to optimize a forging process.

To move forward with the present research, the model of the press and the model of the tools could be dissociated to gain more flexibility in the model's definition. Moreover, a strong coupling between the FE forging software and the dynamic model could be realized.

Acknowledgements The authors gratefully acknowledge the contributions of Jean Francois Mull, Ludovic Freund (design, experiments analysis), Sébastien Burgun, Daniel Boehm, Stéphane Mathieu, and Alexandre Fendler (technical support in the realization of the experimental protocols).

Author contribution All authors contributed to the study conception and design. Material preparation, data collection, and analysis were performed by Heyu Song, Camille Durand, Cyrille Baudouin, and Régis Bigot. The first draft of the manuscript was written by Heyu Song, and all authors commented on previous versions of the manuscript. All authors read and approved the final manuscript.

Funding Open access funding provided by Arts et Metiers Institute of Technology. This work was supported by Manoir Industries. Author Heyu Song has received research support from the China Scholarship Council (CSC).

Declarations

Competing interests The authors declare no competing interests.

References

1. Venet G, Baudouin C, Pondaven C, Bigot R, Balan T (2021) Parameter identification of 42CrMo4 steel hot forging plastic flow behaviour using industrial upsetting presses and finite element simulations. Int J Mater Form 14(5):929–945. https://doi.org/10.1007/s12289-020-01609-1
2. Partovi A, Wang H, Sadeghi B, Wu P (2023) A machine learning approach for determination of coefficient of friction from ring compression test. Tribol Int 180:108198. https://doi.org/10.1016/j.triboint.2022.108198
3. Altan T (Ed.) (2005) Cold and hot forging: fundamentals and applications. Materials Park, ASM International, Ohio
4. Durand C, Bigot R, Baudouin C (2018) Contribution to characterization of metal forming machines: application to screw presses. Procedia Manuf 15:1024–1032. https://doi.org/10.1016/j.promfg.2018.07.391
5. Brecher C, Esser M, Witt S (2009) Interaction of manufacturing process and machine tool. CIRP Ann 58(2):588–607. https://doi.org/10.1016/j.cirp.2009.09.005
6. Volk W et al (2019) Models and modelling for process limits in metal forming. CIRP Ann 68(2):775–798. https://doi.org/10.1016/j.cirp.2019.05.007
7. Ou H, Armstrong CG (2006) Evaluating the effect of press and die elasticity in forging of aerofoil sections using finite element simulation. Finite Elem Anal Des 42(10):856–867. https://doi.org/10.1016/j.finel.2006.01.006
8. Arentoft M, Wanheim T (2005) A new approach to determine press stiffness. CIRP Ann 54(1):265–268. https://doi.org/10.1016/S0007-8506(07)60099-7
9. Behrens B-A, Brecher C, Hork M, Werbs M (2007) New standardized procedure for the measurement of the static and dynamic properties of forming machines. Prod Eng 1(1):31–36. https://doi.org/10.1007/s11740-007-0005-0
10. Krušič V, Arentoft M, Mašera S, Pristovšek A, Rodič T (2011) A combined approach to determine workpiece-tool-press deflections and tool loads in multistage cold-forging. J Mater Process Technol 211(1):35–42. https://doi.org/10.1016/j.jmatprotec.2010.08.020
11. Kroiß T, Engel U, Merklein M (2013) Comprehensive approach for process modeling and optimization in cold forging considering interactions between process, tool and press. J Mater Process Technol 213(7):1118–1127. https://doi.org/10.1016/j.jmatprotec.2012.09.004
12. Swidergal K et al (2015) Experimental and numerical investigation of blankholder's vibration in a forming tool: a coupled

MBS-FEM approach. Prod Eng 9(5):623–634. https://doi.org/10.1007/s11740-015-0640-9
13. Zheng E, Zhou X (2014) Modeling and simulation of flexible slider-crank mechanism with clearance for a closed high speed press system. Mech Mach Theory 74:10–30. https://doi.org/10.1016/j.mechmachtheory.2013.11.015
14. El Hifnawy L, Novak M (1984) Response of hammer foundations to pulse loading. Int J Soil Dyn Earthq Eng 3(3):124–132. https://doi.org/10.1016/0261-7277(84)90042-1
15. Chehab AG, El Naggar MH (2003) Design of efficient base isolation for hammers and presses. Soil Dyn Earthq Eng 23(2):127–141. https://doi.org/10.1016/S0267-7261(02)00157-4
16. Kunadharaju R, Borthakur A (2017) Analysis and design of foundation systems to control the vibrations due to forging impact hammer. J Struct Eng India 44:404–413
17. Hawryluk M, Ziemba J (2017) Possibilities of application measurement techniques in hot die forging processes. Meas J Int Meas Confed 110:284–295. https://doi.org/10.1016/j.measurement.2017.07.003
18. Galdos L, Sáenz De Argandoña E, Herrero N, Ongay M, Adanez J, Sanchez M (2014) The calibration of high energy-rate impact forging hammers by the copper-column upsetting method and high speed camera measurements. Key Eng Mater 611–612:173–177. https://doi.org/10.4028/www.scientific.net/KEM.611-612.173
19. Chen R et al (2019) A stereo-vision system for measuring the ram speed of steam hammers in an environment with a large field of view and strong vibrations. Sensors 19(5):996. https://doi.org/10.3390/s19050996
20. Alimov A, Härtel S, Gardill M, Knaack M, Buhl J (2023) Acquisition of ram tilting and frame stretching with radar sensors during hot forging. WT Werkstattstech 113(10):425–431. https://doi.org/10.37544/1436-4980-2023-10-47
21. Groche P, Hohmann J, Übelacker D (2019) Overview and comparison of different sensor positions and measuring methods for the process force measurement in stamping operations. Meas J Int Meas Confed 135:122–130. https://doi.org/10.1016/j.measurement.2018.11.058
22. Saberi S, Fischer J, Stockinger M, Tikal R, Afsharnia R (2021) Theoretical and experimental investigations of mechanical vibrations of hot hammer forging. Int J Adv Manuf Technol 114(9):3037–3045. https://doi.org/10.1007/s00170-021-07061-y
23. Durand C, Freund L, Baudouin C, Bigot R, Guérin J-D (2021) Comparison of different sensor technologies to monitor a forging process. ESAFORM 2021. https://doi.org/10.25518/esaform21.1475
24. Dao M, Lu L, Shen YF, Suresh S (2006) Strength, strain-rate sensitivity and ductility of copper with nanoscale twins. Acta Mater 54(20):5421–5432. https://doi.org/10.1016/j.actamat.2006.06.062
25. Mull J-F, Durand C, Baudouin C, Bigot R (2020) A new tailored solution to predict blow efficiency and energy consumption of hammer-forging machines. Int J Adv Manuf Technol 111(7–8):1941–1954. https://doi.org/10.1007/s00170-020-06237-2
26. Watermann D (1962) Bestimmung des Arbeitsvermögens von Hämmern und Pressen mit Kupfer-Zylindern. Schmiedetechnische Mitt 2:95–101
27. Gavrus A, Francillette H, Pham DT (2012) An optimal forward extrusion device proposed for numerical and experimental analysis of materials tribological properties corresponding to bulk forming processes. Tribol Int 47:105–121. https://doi.org/10.1016/j.triboint.2011.10.013
28. Ghassemali E, Tan M-J, Jarfors AEW, Lim SCV (2013) Progressive microforming process: towards the mass production of microparts using sheet metal. Int J Adv Manuf Technol 66(5):611–621. https://doi.org/10.1007/s00170-012-4352-4
29. Zhang D-W, Ou H (2016) Relationship between friction parameters in a Coulomb-Tresca friction model for bulk metal forming. Tribol Int 95:13–18. https://doi.org/10.1016/j.triboint.2015.10.030
30. Yoo YH, Yang DY (1997) Finite element modelling of the high-velocity impact forging process by the explicit time integration method. J Mater Process Technol 63(1–3):718–723. https://doi.org/10.1016/S0924-0136(96)02713-6
31. Wang Z, Suzuki T (2018) Friction law in dry metal forming of materials with work hardening. Procedia Manuf 15:475–480. https://doi.org/10.1016/j.promfg.2018.07.253
32. Tobias SA (1985) Survey of the development of petro-forge forming machines. Int J Mach Tool Des Res 25(2):105–197. https://doi.org/10.1016/0020-7357(85)90091-5
33. Vajpayee S, Sadek MM, Tobias SA (1979) The efficiency and clash load of impact forming machines to the second order of approximation. Int J Mach Tool Des Res 19(4):237–252. https://doi.org/10.1016/0020-7357(79)90013-1
34. Chamouard A (1970) Estampage et forge: Tome 3, Technologie générale et forge